Medicine®

OPEN

# Diagnostic value of thallium-201 myocardial perfusion IQ-SPECT without and with computed tomography-based attenuation correction to predict clinically significant and insignificant fractional flow reserve
## A single-center prospective study

Haruki Tanaka, MD, PhD[a,*], Teruyuki Takahashi, BSc[b], Norihiko Ohashi, MD, PhD[c], Koichi Tanaka, MD, PhD[a], Takenori Okada, MD, PhD[c], Yasuki Kihara, MD, PhD[d]

**Abstract**

The aim of this study was to clarify the predictive value of fractional flow reserve (FFR) determined by myocardial perfusion imaging (MPI) using thallium (TI)-201 IQ-SPECT without and with computed tomography-based attenuation correction (CT-AC) for patients with stable coronary artery disease (CAD).

We assessed 212 angiographically identified diseased vessels using adenosine-stress TI-201 MPI-IQ-SPECT/CT in 84 consecutive, prospectively identified patients with stable CAD. We compared the FFR in 136 of the 212 diseased vessels using visual semiquantitative interpretations of corresponding territories on MPI-IQ-SPECT images without and with CT-AC.

FFR inversely correlated most accurately with regional summed difference scores (rSDS) in images without and with CT-AC ($r = -0.584$ and $r = -0.568$, respectively, both $P < .001$). Receiver-operating characteristics analyses using rSDS revealed an optimal FFR cut-off of $<0.80$ without and with CT-AC. Although the diagnostic accuracy of FFR $<0.80$ did not significantly differ, FFR $\geq 0.82$ was significantly more accurate with, than without CT-AC. Regions with rSDS $\geq 2$ without or with CT-AC predicted FFR $<0.80$, and those with rSDS $\leq 1$ without and with CT-AC predicted FFR $\geq 0.81$, with 73% and 83% sensitivity, 84% and 67% specificity, and 79% and 75% accuracy, respectively.

Although limited by the sample size and the single-center design, these findings showed that the IQ-SPECT system can predict FFR at an optimal cut-off of $<0.80$, and we propose a novel application of CT-AC to MPI-IQ-SPECT for predicting clinically significant and insignificant FFR even in nonobese patients.

**Abbreviations:** 3D-OSCGM = 3-dimensional ordered subset conjugate gradient modification, AC = attenuation correction, AUC = area under the curve, CAD = coronary artery disease, CAG = coronary angiography, CI = confidence interval, CT = computed tomography, CT-AC = computed tomography-based attenuation correction, CZT = cadmium-zinc-telluride, DLP = dose-length product, ECG = electrocardiography, FFR = fractional flow reserve, HLA = horizontal long-axis, IDI = integrated discrimination improvement, LAD = left anterior descending artery, MPI = myocardial perfusion imaging, MPR = myocardial perfusion reserve, NRI = net reclassification improvement, QCA = quantitative coronary angiography, QPS = quantitative perfusion single-photon emission computed tomography, ROC = receiver-operating characteristics, rSDS = regional summed difference score, rSRS = regional summed rest score, rSSS = regional summed stress score, SA = short-axis, SD = standard deviation, SPECT = single-photon emission computed tomography, TI-201 = thallium-201, VLA = vertical long-axis.

**Keywords:** coronary artery disease, IQ-SPECT, attenuation artifact, predictive value

# 1. Introduction

Both invasively measurable fractional flow reserve (FFR)[1,2] and noninvasive myocardial perfusion imaging (MPI) using single-photon emission computed tomography (SPECT)[3,4] are essential tools with which to diagnose the functional severity of coronary artery disease (CAD), stratify risk, and decide management strategies for patients with suspected or known stable CAD. Although FFR and MPI-SPECT findings fundamentally differ, we previously developed a model of FFR prediction based on quantitative thallium (Tl)-201 MPI-SPECT findings and found that attenuation artifacts might represent an obstacle in the modeling process.[5] Attenuation artifacts arising from soft-tissue inhomogeneous photon absorption cause a reduction in the specificity of detecting CAD using MPI-SPECT.[6] Thus, attenuation correction (AC) of MPI-SPECT images is recommended for clinical practice in the United States[7] and Europe.[8] Today, the most popular method of AC includes x-ray computed tomography (CT) to generate linear attenuation coefficient maps (μ maps).[9] Several studies have shown that CT-based AC (CT-AC) can improve specificity without reducing sensitivity, which consequently improve detection, and thus the accuracy of diagnosing CAD.[10,11] However, all of these findings were derived using conventional collimators and γ-cameras with angiographic findings as the reference standard.

Recent technological advances in MPI-SPECT have led to the introduction of the IQ-SPECT system that includes a multifocal collimator to magnify the heart with cardiocentric and 3-dimensional iterative SPECT reconstruction.[12] It is characterized by rapid image acquisition, and the quality of the SPECT images is high,[13,14] even when using Tl-201 without or with AC.[15–18] However, the relationship between FFR and IQ-SPECT findings, and the effects of CT-AC on these findings remain unknown. The present study aimed to clarify the diagnostic value of Tl-201 MPI-IQ-SPECT without and with CT-AC to predict clinically significant and insignificant FFR in patients with stable CAD using FFR as the reference standard.

# 2. Methods

## 2.1. Study design and participants

This single-center prospective study evaluated the diagnostic accuracy of adenosine-stress Tl-201 MPI-IQ-SPECT images without and with CT-AC, using FFR as the reference standard. Japanese patients who were diagnosed with suspected or known CAD and indicated for invasive coronary angiography (CAG), between April 2013 and March 2014 at the Department of Cardiology, Hiroshima Red Cross and Atomic-bomb Survivors Hospital, Hiroshima, Japan, were recruited. Patients with acute coronary syndrome, previous coronary artery bypass surgery, paced rhythm and contraindications against adenosine, and patients who withheld written informed consent to participate in the present study were excluded. A total of 84 patients (52 males and 32 females) were included in the final analysis. All participants provided written informed consent. Patients were assessed by adenosine-stress Tl-201 MPI-IQ-SPECT/CT, and FFR was measured within 4 weeks without a significant intervening event. MPI-IQ-SPECT images were interpreted by comparing measured FFR and visual perfusion scores at the corresponding vascular territory without or with CT-AC. The Ethics Review Board at the Hiroshima Red Cross and Atomic-bomb Survivors Hospital approved the study protocol (Approval No. 204).

## 2.2. Coronary lesions

We identified 212 diseased vessels with angiographically suspected flow limitation. We incorporated all potentially flow-limiting coronary lesions including those with ≥50% (n = 178) diameter stenosis determined by quantitative coronary angiography (QCA) and with <50% (n = 34), but with visually interpreted morphological abnormalities that might cause flow limitations such as in-stent or stent marginal (n = 8), hazy (n = 9), ulcerated (n = 5), or diffuse (>20 mm, n = 11) lesions and kinked motion (n = 1). The guidewire could not pass through 76 of the diseased vessels because of lesions being located in branches (n = 26), chronic total obstruction (n = 22), distal and imposed technical difficulties (n = 20), being diffuse (n = 5), tortuous (n = 2), or having an anomalous coronary origin (n = 1). We thus measured FFR in 136 (64.2%) of the 212 diseased vessels.

## 2.3. IQ-SPECT/CT image acquisition and reconstruction protocol

All patients were assessed using a 1-day stress/rest Tl-201 MPI-IQ-SPECT/CT protocol. Stress was induced in supine patients by a continuous 6-minute infusion of adenosine (140 μg/kg/min) through a brachial vein and an injection of 111 MBq (3 mCi) of Tl-201 three minutes after starting the adenosine infusion. Rest images were acquired from supine patients 4 hours later. Medications were discontinued 24 hours before, and caffeinated foods or beverages were not consumed for at least 12 hours before starting the study. Images were acquired using Symbia T6 dual-head hybrid SPECT/CT cameras equipped with an IQ-SPECT system[12] (Siemens Medical Solutions, Munich, Germany) under the following parameters: 128 × 128 matrix, 208 degree rotation with 34 views and a 17-second scan duration per view. A 20% acceptance window was located only around the 70 keV photon peak. All images were reconstructed using a 3-dimensional ordered subset conjugate gradient modification (3D-OSCGM) with 30 iterations, 1 subset, and a 7.0-mm Gaussian filter. Nonenhanced CT images were also acquired using the 6-slice CT scanner of the Symbia T6 to develop μ maps that were independently optimized for a Tl-201 photon peak of 70 keV in stress and rest images under the following parameters: no electrocardiography (ECG) triggering, slice thickness, 5.0 mm; tube voltage, 130 kV; tube current, 13 mA. A dose-length product (DLP) was established at 35 mGy·cm per CT image (totally 70 mGy·cm per MPI-IQ-SPECT/CT study). Images with CT-AC were reconstructed based on μ maps, and processed using quantitative perfusion SPECT (QPS) software (Cedars-Sinai Medical Center, Los Angeles, CA). All images were acquired without missing data.

## 2.4. Coronary angiography and FFR measurement

Three experienced cardiologists without knowledge of the MPI-IQ-SPECT/CT findings implemented invasive CAG and measured FFR within 4 weeks of completing the MPI-IQ-SPECT/CT study. All medications were discontinued 24 hours before, and the patients refrained from consuming foods or beverages containing caffeine for at least 12 hours before starting the study. We measured FFR using a standard 5-F diagnostic or 6-F guiding catheter without a side hole. A pressure transducer was standardized at zero, 5 cm below the sternum. The severity of coronary lesions was determined using QCA and CAAS5 software (Pie Medical Imaging, Maastricht, Belgium) and FFR was measured using a PressureWire Certus intracoronary

pressure sensor-tipped guidewire (St. Jude Medical, Uppsala, Sweden). An intracoronary bolus of isosorbide dinitrate (0.5 mg) was administered, then the pressure-monitoring wire was calibrated and advanced to the tip of the catheter to equalize pressure and introduced into the farthest distal part of identified coronary lesions. The FFR was derived online using a Radi Analyzer Unit (St. Jude Medical) from the ratio of a 5-beat average of mean distal coronary pressure to proximal aortic pressure at maximal steady state hyperemia. Maximal hyperemia was achieved via a continuous infusion of adenosine triphosphate through the brachial, femoral, or internal jugular vein from a weight-adjusted initial dose of 120 μg/kg/min and titrated to 210 μg/kg/min in 30 μg/kg/min increments for 3 minutes each until FFR reached a steady state. Up-titration proceeded in the event of anginal chest pain, extensive ECG changes, extreme hypotension (systolic blood pressure <70 mmHg) or severe bradycardia (<40 bpm). The lowest FFR was defined as representative of a diseased vessel. No adverse events were associated with invasive CAG and FFR measurement.

### 2.5. Visual perfusion analysis

Supplemental Figure (see Figure, Supplemental Digital Content 1, which demonstrates left ventricular segmentation, http://links.lww.com/MD/C26) shows visual interpretation of MPI-IQ-SPECT/CT that was based on short (SA), vertical (VLA), and horizontal long-axis (HLA) tomograms divided into 17 segments.[19] Two independent experienced observers scored segmental uptake using a scale from 0 to 4, (0, normal; 1, mildly reduced; 2, moderately reduced; 3, severely reduced and 4, absent).[20] The interpreters were blinded to the clinical information of the patients including medical history, CAG, and FFR findings. However, all MPI-IQ-SPECT/CT image data including raw projections, gated stress and rest images, images without or with CT-AC, and automated semiquantitative scores determined by QPS software were taken into account during visual scoring. Intraobserver discrepancies were resolved by consensus. Coronary perfusion territories were basically assigned to default assignments (see Figure, Supplemental Digital Content 1, which demonstrates left ventricular segmentation, http://links.lww.com/MD/C26). A third observer had the option to modify the default assignment of segments to a specific vascular territory according to the CAG findings. Regional summed scores for stress (rSSS) and rest (rSRS) were then calculated by summing the respective segmental scores. Regional summed difference scores (rSDS) were calculated as differences between rSSS and rSRS.

### 2.6. Statistical analysis

Continuous and categorical variables are expressed as means ± standard deviation (SD) and as ratios (%), respectively. Continuous variables between groups were compared using unpaired $t$ tests or nonparametric Mann–Whitney tests. Unpaired and paired categorical variables were compared using $\chi^2$ tests and McNemar tests, respectively. Receiver-operating characteristic (ROC) curves were developed based on the outcomes of univariate logistic regression analyses and statistically optimal cut-offs for ROC curves were determined at a predicted value of 0.50 in the respective logistic regression model. Pairs of ROC curves were assessed by comparing areas under the curves (AUC) and diagnostic accuracy at a statistical optimal cut-off. Two logistic regression models were also compared by net reclassification,[21] at the same predicted value. We considered both statistical parameters, net reclassification improvement, and integrated discrimination improvement, in which values with $P$ <.05 were taken to indicate statistically significant improvement. Comparisons of AUC between paired ROC curves and net reclassifications were assessed using the R 3.0.2 statistical software package with pROC and PredictABEL (The R Foundation for Statistical Computing, http://www.r-project.org/) and other data were statistically analyzed using SPSS 21.0 for Windows software (SPSS Inc, Chicago, IL).

## 3. Results

### 3.1. Characteristics of study population and diseased vessels

Tables 1 and 2 respectively describe the characteristics of the study population and the 136 diseased vessels in which FFR was measured.

### 3.2. Relationship between visual perfusion scores on IQ-SPECT/CT images and FFR

Table 3 summarizes correlations between visual perfusion scores and FFR. Among the tested parameters, rSDS inversely correlated the most accurately with FFR that was considered statistically moderate without and with CT-AC. Thus, subsequent analyses proceeded with focus on rSDS.

### 3.3. Optimal FFR cut-off determined using rSDS

Figure 1 shows the results of ROC analyses based on univariate logistic regression analyses at various FFR cut-offs using rSDS. The AUC was the largest at FFR <0.80 or ≥0.80 in images without and with CT-AC. Although the AUC did not significantly

| Table 1 | |
|---|---|
| **Characteristics of patients (n = 84).** | |
| **Parameter** | **Value** |
| Male sex | 52 (61.9) |
| Age, y | 73.5 ± 9.1 |
| Body mass index, kg/m² | 24.6 ± 3.8 |
| Medical history | |
|   Diabetes | 44 (52.4) |
|   Hypertension | 77 (91.7) |
|   Dyslipidemia | 70 (83.3) |
|   Obesity (BMI ≥25.0 kg/m²) | 36 (42.9) |
|   Previous myocardial infarction | 24 (28.6) |
|   Previous percutaneous coronary intervention | 36 (42.9) |
| Quantitative coronary angiography findings (%diameter stenosis ≥50%) | |
|   LM | 6 (7.1) |
|   LAD | 63 (75.0) |
|   LCX | 39 (46.4) |
|   RCA | 52 (61.9) |
|   LM disease | 1 (1.2) |
|   LM + 1-VD | 1 (1.2) |
|   LM + 2-VD | 1 (1.2) |
|   LM + 3-VD | 3 (3.6) |
|   No vessel disease | 5 (6.0) |
|   1-VD | 22 (26.2) |
|   2-VD | 33 (39.3) |
|   3-VD | 18 (21.4) |

Data are shown as means ± SD or n (%). BMI = body mass index, LAD = left anterior descending artery, LCX = left circumflex artery, LM = left main, RCA = right coronary artery, VD = vessel disease.

## Table 2

**Characteristics of vessels in which FFR was measured (n = 136).**

| Characteristics | | FFR <0.80 | FFR ≥0.80 |
|---|---|---|---|
| Number of vessels | | 62 | 74 |
| FFR findings | | | |
| Measured coronary arteries | | | |
| LAD | | 38 (61.3)* | 31 (41.9) |
| LCX | | 11 (17.7) | 21 (28.4) |
| RCA | | 13 (21.0) | 22 (29.7) |
| Previous myocardial infarcted artery | | 10 (16.1) | 6 (8.1) |
| Adenosine triphosphate, μg/kg/min | | 168 ± 18* | 181 ± 16 |
| FFR | | 0.63 ± 0.13* | 0.89 ± 0.06 |
| Visual perfusion scores | CT-AC | | |
| rSSS | − | 4.8 ± 5.6* | 1.3 ± 2.7 |
| rSRS | − | 2.3 ± 4.0* | 0.9 ± 2.5 |
| rSDS | − | 2.6 ± 3.0* | 0.4 ± 0.9 |
| rSSS | + | 5.0 ± 5.8* | 1.1 ± 2.3 |
| rSRS | + | 1.9 ± 3.8* | 0.7 ± 2.1 |
| rSDS | + | 3.1 ± 3.7* | 0.5 ± 0.9 |

Data are shown as means ± SD or n (%). + = with CT-AC, − = without CT-AC, CT-AC = computed tomography-based attenuation correction, FFR = fractional flow reserve, rSDS = regional summed difference score, rSRS = regional summed rest score, rSSS = regional summed stress score.
* P < .05 vs. FFR ≥0.80.



**Figure 1.** Comparisons of AUC and diagnostic accuracy between without and with CT-AC determined by ROC analyses based on univariate logistic regression models using regional summed difference score at various FFR cut-offs. *Significantly reclassified by net reclassifications (Table 4A and B). AUC = area under the curve, CT-AC = computed tomography-based attenuation correction, FFR = fractional flow reserve, ROC = receiver operating characteristics.
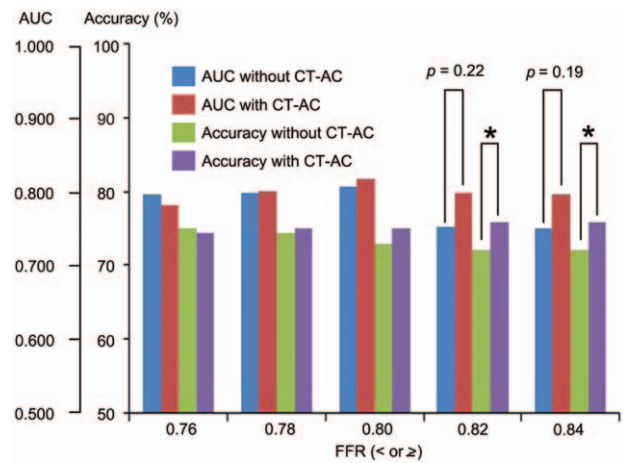
differ between without and with CT-AC at any tested FFR cut-off, the AUC and the diagnostic accuracy tended to be larger and better, respectively, at FFR (< or ≥) 0.82 and 0.84 with, than without CT-AC. Net reclassification revealed that the model with CT-AC significantly reclassified 20% of FFR <0.82 and <0.84, and 25% of FFR ≥0.82 and ≥0.84 predicted based on the model without CT-AC (Table 4A and B), whereas differences were not clearly significant at other FFR cut-offs. These results indicated that the differences in diagnostic accuracy between images without and with CT-AC at FFR cut-offs of (< or ≥) 0.82 and (< or ≥) 0.84 were significant (Fig. 1). Findings from a regional comparison of the diagnostic value of CT-AC using rSDS were similar (see Table, Supplemental Digital Content 2, which demonstrates regional comparison of FFR prediction without and with CT-AC using rSDS and net reclassification, http://links.lww.com/MD/C26). Net reclassification showed that CT-AC significantly reclassified 38% of FFR <0.83 predicted in the absence of CT-AC in the left anterior descending artery (LAD) region at FFR ≥0.83, and 17% of FFR <0.84, and 14% of FFR ≥0.84 predicted in the absence of CT-AC in the non-LAD region at FFR ≥0.84.

## Table 4

**Ability of CT-AC to predict FFR determined using rSDS and net reclassification.**

**A. FFR ≥0.82**

| FFR predicted without CT-AC | FFR predicted with CT-AC | | |
|---|---|---|---|
| | <0.82 | ≥0.82 | %Reclassified |
| FFR <0.82 (n=71) | | | |
| <0.82 | 43 | 6 | 12 |
| ≥0.82 | 11 | 11 | 50 |
| FFR ≥0.82 (n=65) | | | |
| <0.82 | 9 | 7 | 44 |
| ≥0.82 | 7 | 42 | 14 |
| Combined data (n=136) | | | |
| <0.82 | 52 | 13 | 20 |
| ≥0.82 | 18 | 53 | 25 |

NRI (95%CI), 0.819 (0.529–1.109), P=0. IDI (95%CI), 0.087 (0.023–0.151), P=.008.

**B. FFR ≥0.84**

| FFR predicted without CT-AC | FFR predicted with CT-AC | | |
|---|---|---|---|
| | <0.84 | ≥0.84 | %Reclassified |
| FFR <0.84 (n=77) | | | |
| <0.84 | 45 | 7 | 13 |
| ≥0.84 | 12 | 13 | 48 |
| FFR ≥0.84 (n=59) | | | |
| <0.84 | 7 | 6 | 46 |
| ≥0.84 | 6 | 40 | 13 |
| Combined data (n=136) | | | |
| <0.84 | 52 | 13 | 20 |
| ≥0.84 | 18 | 53 | 25 |

NRI (95% CI), 0.872 (0.590–1.154), P=0. IDI (95% CI), 0.099 (0.038–0.161), P=.001.

CI = confidence interval, CT-AC = computed tomography-based attenuation correction, FFR = fractional flow reserve, IDI = integrated discrimination improvement, NRI = net reclassification improvement, rSDS = regional stress difference score.

## Table 3

**Summary of correlations between visual perfusion scores and FFR (n = 136).**

| Visual perfusion score | CT-AC | Correlation coefficient | P |
|---|---|---|---|
| rSDS | − | −0.584 | <.001 |
| rSDS | + | −0.568 | <.001 |
| rSSS | + | −0.544 | <.001 |
| rSSS | − | −0.489 | <.001 |
| rSRS | + | −0.280 | .001 |
| rSRS | − | −0.271 | .001 |

+ = with CT-AC, − = without CT-AC, CT-AC = computed tomography-based attenuation correction, FFR = fractional flow reserve, rSDS = regional summed difference score, rSRS = regional summed rest score, rSSS = regional summed stress score.

### 3.4. Practical optimal rSDS cut-off to predict clinically significant and insignificant FFR

Figure 2 shows the ROC curves at FFR <0.80 (A), ≤0.80 (B), ≥0.81 (C), and ≥0.82 (D) without and with CT-AC using rSDS, and the statistical optimal rSDS cut-off to predict the indicated FFR. The findings suggest that the practical optimal rSDS cut-off to predict FFR <0.80 and ≤0.80 was ≥ 2, whereas those to predict FFR ≥0.81 and ≥0.82 were ≤1 and 0, respectively, in images without and with CT-AC.

### 3.5. Diagnostic performance of combined interpretation of IQ-SPECT images without and with CT-AC to predict clinically significant and insignificant FFR

Individual applications without or with CT-AC for predicting clinically significant and insignificant FFR might be limited because of the low sensitivity to predict FFR <0.80 (Fig. 3A) and the low specificity to predict FFR ≥0.81 (Fig. 3B). However, interpretation of the combined outcomes generated without and with CT-AC revealed that regions with rSDS ≥2 without or with CT-AC predicted FFR <0.80, and those with rSDS ≤1 without and with CT-AC predicted FFR ≥0.81 with 73% and 83%, sensitivity, 84% and 67%, specificity, and 79% and 75%, accuracy, respectively (Fig. 3A and B). The diagnostic accuracy of the former criteria was decreased at FFR ≤0.80 compared with that at FFR <0.80 (see Figure, Supplemental Digital Content 3, which demonstrates diagnostic performance of combined interpretation of IQ-SPECT images without and with CT-AC to predict FFR ≤0.80, http://links.lww.com/MD/C26).

## 4. Discussion

FFR is an established reference standard for the invasive assessment of CAD severity and for making clinical decisions.[1,2]
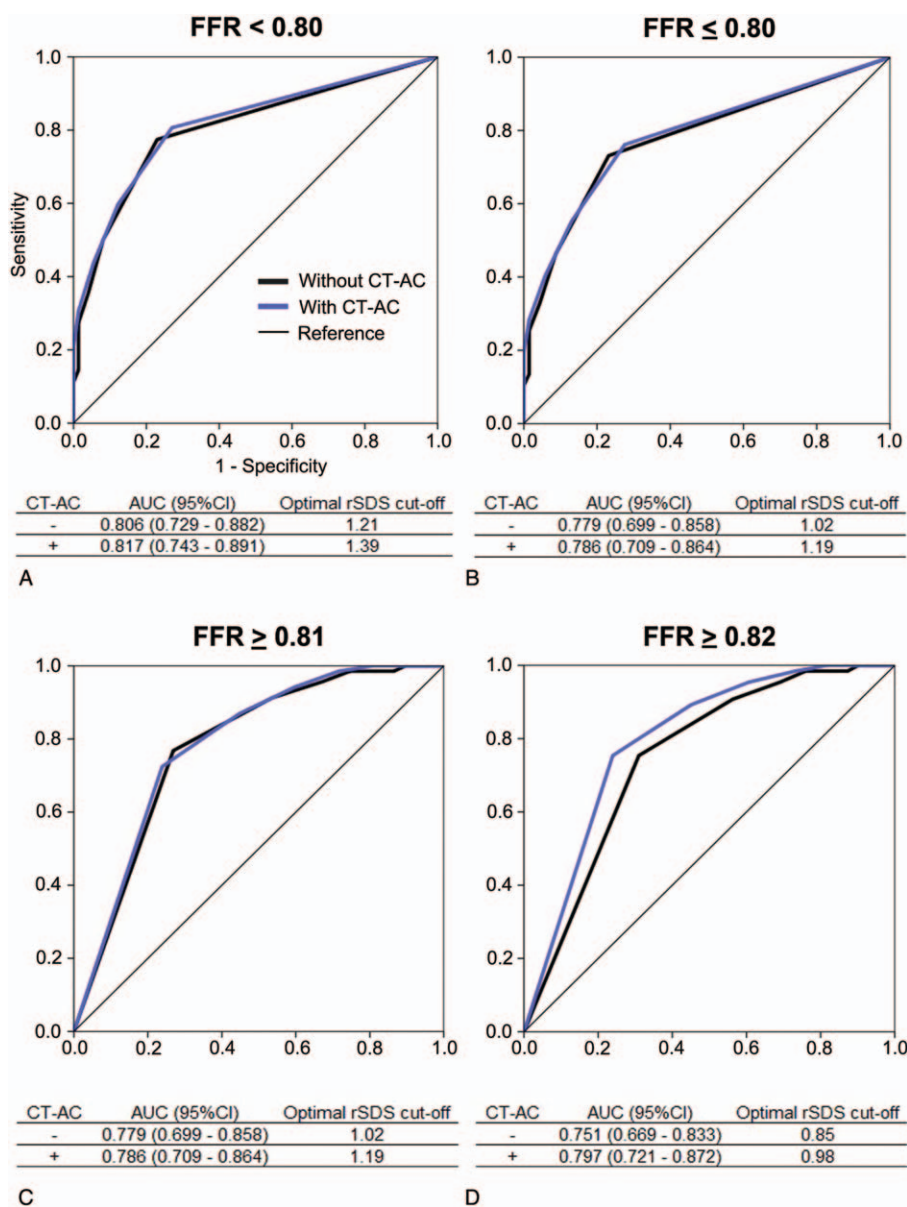


**Figure 2.** Comparison of ROC curves and statistically optimal rSDS cut-offs between without and with CT-AC to predict FFR <0.80 (A), ≤0.80 (B), ≥0.81 (C), and ≥0.82 (D). AUC=area under the curve, CI=confidence interval, CT-AC=computed tomography-based attenuation correction, FFR=fractional flow reserve, ROC=receiver operating characteristics, rSDS=regional summed difference score.
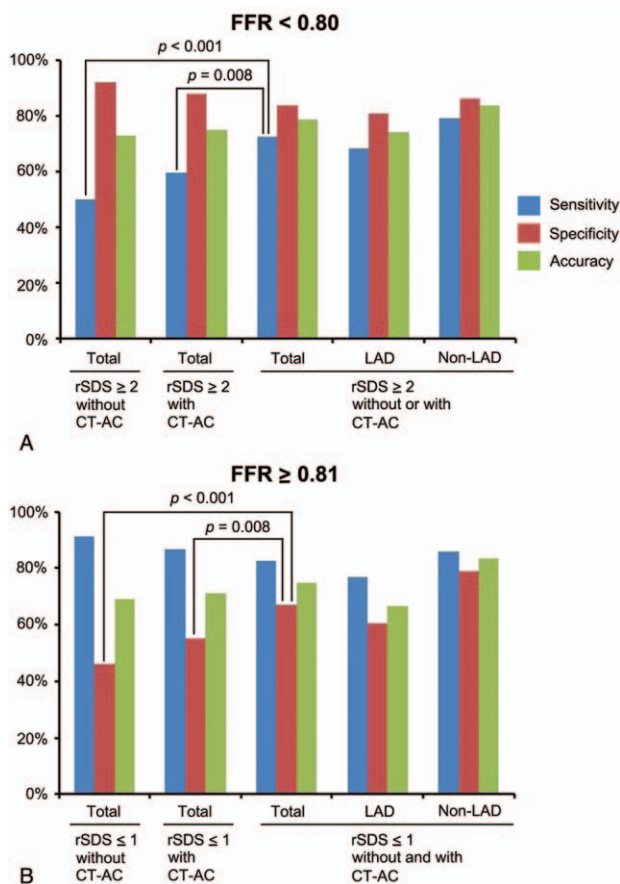
**Figure 3.** Diagnostic performance of combined interpretations of IQ-SPECT images without and with CT-AC to predict FFR <0.80 (A) and ≥0.81 (B). P values assessed using McNemar tests. CT-AC=computed tomography-based attenuation correction, FFR=fractional flow reserve, LAD=left anterior descending artery, rSDS=regional summed difference score.

The FFR value of <0.75 has been validated for identifying reversible ischemia defined by noninvasive stress testing including MPI-SPECT, dobutamine-stress echocardiography, and exercise stress testing,[22–24] whereas that of ≤0.80 is widely accepted as being appropriate to guide clinical decisions regarding revascularization for favorable prognostic outcomes.[1,2,25] The FFR value of <0.75 is a consensus threshold validated by three or more modalities; it does not necessarily equal a statistically identified optimal cutoff value or detectable limit determined by a single modality. In addition, advances in MPI-SPECT technology,[12] during the past 2 decades including the IQ-SPECT system and the cadmium-zinc-telluride (CZT) semiconductor camera, provide high-quality images as a result of rapid, highly sensitive acquisition.[13–18,26,27] The optimal FFR cut-off determined by such modalities without and with CT-AC remains unknown.

### 4.1. Regional SDS most accurately correlates with FFR

Considering direct correlations between visual perfusion scores of Tl-201 MPI-IQ-SPECT and FFR, the moderately inverse correlation between rSDS and FFR was the most accurate both without and with CT-AC. These results agree with previous findings in which FFR correlated with reversible myocardial perfusion abnormalities identified by visual,[22,28–30] visual semiquantitative,[23,24,27,31–38] or automated quantitative,[5,35,39]

MPI-SPECT, and the outcomes of regional myocardial perfusion reserve (MPR) assessed by quantitative dynamic SPECT.[40]

### 4.2. Potential ability of MPI-IQ-SPECT/CT to predict FFR cut-off of <0.80

Regardless of the presence or absence of CT-AC, the AUC derived from ROC analyses based on univariate logistic regression analyses using rSDS, was the largest at an FFR cut-off of <0.80, which agrees with our previous findings derived from quantitative Tl-201 MPI-IQ-SPECT analysis.[5] The AUC was also slightly higher than the validated FFR of <0.75,[22,41] and reported values between 0.73 and 0.78,[23] that were primarily derived using conventional collimators and γ-cameras. Although limited by a relatively small sample size and the absence of a direct comparison between conventional MPI-SPECT modalities and the IQ-SPECT system, the present findings might nevertheless reflect the improved image quality of the IQ-SPECT system.

### 4.3. Effect of CT-AC on MPI-IQ-SPECT findings to predict FFR

AC techniques in MPI-SPECT are recommended and several studies using CT-AC have improved the accuracy of diagnosing CAD.[10,11] However, other findings that have been contradictory,[42–44] those of which were derived using angiographic findings as the reference standard. Otherwise, several methods have been proposed for AC, including prone,[6] and ECG-gated SPECT[45] imaging that could serve as an alternative to CT-AC. Taken together with the intention to avoid additional radiation exposure, some clinicians do not generally consider CT-AC, except for significantly obese patients with a body mass index >40.[11] Using FFR as the reference standard in this study, we determined that FFR ≥0.82 was diagnosed significantly more accurately with, than without CT-AC. The findings were similar in both LAD and non-LAD regions and the diagnostic accuracy of FFR <0.80 did not significantly differ between images without and with CT-AC acquired by MPI-IQ-SPECT.

### 4.4. Comparison between MPI-IQ-SPECT/CT findings to predict FFR in the present and previously published studies

Table 5 lists published reports describing studies of the diagnostic value of MPI-SPECT findings to predict FFR that included per-vessel analyses and reanalyses using cross-tabulation. Based upon the findings of these studies, the most recent meta-analysis found that the per-vessel sensitivity and specificity of MPI-SPECT findings mainly acquired using conventional collimators and γ-cameras to diagnose significant FFR are 57% (95% confidence interval [CI]: 49%–64%) and 75% (95%CI: 69%–80%), respectively.[46] Our findings showed that the independent application of rSDS ≥2 to images without or with CT-AC acquired by Tl-201 MPI-IQ-SPECT to predict FFR <0.80 showed sensitivity 50% and 60%, specificity 92% and 88%, and accuracy 73% and 75%, respectively (Fig. 3A). The sensitivity was essentially within the range of the recent meta-analysis,[46] but the specificity was better. Thus, the diagnostic ability of Tl-201 MPI-IQ-SPECT to predict FFR <0.80 using the criterion of rSDS ≥2 regardless of the presence or absence of CT-AC, is at least comparable to that of previous reports using criteria such as rSDS ≥1 or a reversible perfusion defect, derived using

**Table 5**

**Previous reports on diagnostic ability of MPI-SPECT findings to predict FFR in which per-vessel analyses were performed.**

| Author | Patients | Previous MI (%) | MVD (%) | FFR-measured vessels | Tracer | Detector | Collimator | Attenuation correction | FFR cut-off | MPI-SPECT criteria for predicting FFR | Sensitivity (%) | Specificity (%) | Accuracy (%) |
|---|---|---|---|---|---|---|---|---|---|---|---|---|---|
| Chikamori et al[27] | 102 | 30 (29) | 44 (43) | 92 | Tc-99m TF, Tc-99m MIBI | CZT | Multiple pinhole | None | ≤0.80 | Regional SDS ≥1 | 77 | 91 | 84 |
| Tanaka et al[5] | 84 | 24 (29) | 57 (68) | 136 | Tl-201 | Anger | IQ-SPECT | None | <0.80 | Regional stress minus rest TPD ≥1 (%) | 60 | 91 | 76 |
| Ben Bouallègue et al[40] | 23 | 7 (30) | 23 (100) | 26 | Tc-99m TF | CZT | Multiple pinhole | None | <0.80 | Regional MPR <2 | 89 | 82 | 85 |
| Kamiya et al[38] | 25 | 0 (0) | 14 (56) | 71 | Tc-99m TF | Anger | LE. HR. PH. | None | <0.80 | Regional SDS ≥1 | 69 | 79 | 75 |
| Schaap et al[37] | 98 | 0 (0) | 41 (42) | 225 | Tc-99m MIBI | Anger | LE. HR. PH. | CT-based | <0.80 | Equivocal, probably and definitely abnormal MPI findings defined by Abidov et al[20] | 62 | 84 | 76 |
| Jakljević et al[36] | 286 | 0 (0) | N.D. | 286 | Tc-99m MIBI | Anger | LE. AP. PH. | None | <0.80 | Presence of reversible perfusion defect | 82 | 62 | 70 |
| Sahiner et al[35] | 58 | 6 (10) | 25 (43) | 58 (LAD) | Tl-201 | Anger | LE. AP. PH. | None | <0.75 | Regional SSS ≥3 and regional SDS ≥2 | 62 | 89 | 83 |
| | | | | | | | | | | Regional SSS ≥3 | 85 | 84 | 84 |
| Melikian et al[34] | 67 | 0 (0) | 67 (100) | 201 | Tc-99m MIBI | Anger | LE. HR. PH. | None | ≤0.80 | Regional SDS ≥1 | 47 | 80 | 67 |
| Förster et al[33] | 72 | N.D. | 72 (100) | 93 | Tc-99m MIBI | Anger | LP. FP. PH. | Gd-153 line sorce-based | <0.75 | Regional SDS ≥1 | 62 | 90 | 84 |
| Ragosta et al[32] | 36 | 7 (19) | 36 (100) | 88 | Tc-99m MIBI | Anger | LE. HR. PH. | N.D. | ≤0.75 | Presence of reversible perfusion defect | 59 | 85 | 69 |
| Hacker et al[31] | 50 | 11 (22) | 40 (80) | 50 | Tc-99m MIBI | Anger | LP. FP. PH. | Gd-153 line source-based | <0.75 | Regional SDS ≥1 | 71 | 73 | 72 |
| | | | | | | | | | | Regional SSS ≥3 | 82 | 88 | |
| Erhard et al[24] | 47 | 24 (54) | 40 (85) | 47 | Tc-99m MIBI | Anger | LE. PH. | N.D. | ≤0.75 | Presence of reversible perfusion defect | 63 | 84 | 77 |
| Morishima et al[39] | 20 | 16 (80) | 4 (20) | 20 | Tc-99m MIBI | Anger | LE. HR. PH. | N.D. | <0.75 | Absence of ATP-induced increase in regional Tc-99m sestamibi direct counts | 100 | 73 | 85 |
| Rieber et al[30] | 48 | 11 (23) | 41 (85) | 43 | Tc-99m MIBI | Anger | N.D. | Gd-153 line source-based | ≤0.75 | Presence of reversible perfusion defect | 69 | 87 | 81 |
| Yanagisawa et al[23] | 165 | 70 (42) | 40 (24) | 194 | Tl-201 | Anger | LE. HR. PH. | N.D. | <0.75 | Presence of reversible perfusion defect | 72 | 80 | 76 |
| Caymaz et al[29] | 30 | 0 (0) | 5 (17) | 40 | Tl-201 | Anger | LE. AP. PH. | N.D. | <0.75 | Presence of reversible perfusion defect | 100 | 90 | 95 |
| Pijls et al[22] | 45 | 0 (0) | N.D. | 45 | Tl-201 | Anger | LE. MR. PH. | N.D. | <0.75 | Presence of reversible perfusion defect | 57 | 96 | 78 |
| Tron et al[28] | 62 | 11 (18) | 29 (47) | 70 | Tc-99m MIBI, Tl-201 | Anger | HR. PH. | N.D. | ≤0.69 | Presence of reversible perfusion defect | 71 | 63 | 67 |
| Tanaka et al (this study) | 84 | 24 (29) | 57 (68) | 136 | Tl-201 | Anger | IQ-SPECT | CT-based | <0.80 | Regional SDS ≥2 without CT-AC | 50 | 92 | 73 |
| | | | | | | | | | | Regional SDS ≥2 with CT-AC | 60 | 88 | 75 |
| | | | | | | | | | | Regional SDS ≥2 without or with CT-AC | 73 | 84 | 79 |
| | | | | | | | | | ≥0.81 | Regional SDS ≤1 without and with CT-AC | 83 | 67 | 75 |

AP = all purpose, ATP = adenosine triphosphate, CT-AC = computed tomography-based attenuation correction, CZT = cadmium-zinc-telluride, FFR = fractional flow reserve, FP = fourth power, Gd = gadlinium, HR = high resolution, LAD = left anterior descending artery, LE = low energy, LP = low pass, MI = myocardial infarction, MIBI = sestamibi, MPI = myocardial perfusion imaging, MPR = myocardial perfusion reserve, MR = medium resolution, MVD = multi-vessel disease, N.D. = not described, PH = parallel hole, SDS = summed difference score, SSS = summed stress score, Tc = technetium, TF = tetrofosmin, Tl = thallium, TPD = total perfusion defect.

conventional MPI-SPECT modalities to predict significant FFR ($\leq$0.69–<0.80; Table 5). Otherwise, recent reports using CZT semiconductor camera have demonstrated better diagnostic ability to predict FFR $\leq$0.80 using the criteria of rSDS $\geq$1,[27] and FFR <0.80 with regional MPR <2 derived from dynamic SPECT analysis[40] (sensitivity 77% and 89%, specificity 91% and 81%, and accuracy 84% and 85%, respectively) that are better outcomes than the findings of the present study and the recent meta-analysis.[46] Further investigations using advanced MPI-SPECT/CT modalities including the IQ-SPECT system and the CZT semiconductor camera, are required.

### 4.5. Novel application of CT-AC in MPI-IQ-SPECT for predicting clinically significant and insignificant FFR

Interpretation of the combined outcomes generated without and with CT-AC revealed that regions with rSDS $\geq$2 without or with CT-AC predicted FFR <0.80, whereas those with rSDS $\leq$1 without and with CT-AC predicted FFR $\geq$0.81 with sensitivity, 73% and 83%, specificity, 84% and 67% and accuracy, 79% and 75%, respectively (Fig. 3A and B, Table 5). Interpretation of the combined outcomes generated without and with CT-AC significantly improved sensitivity and specificity for predicting FFR <0.80 and $\geq$0.81, respectively, compared with independent interpretations of images without or with CT-AC (Fig. 3A and B). Although an FFR cut-off of $\leq$0.80 is validated as the therapeutic reference standard, outcomes were suboptimal with the current criteria to predict FFR $\leq$0.80, compared with those to predict FFR <0.80 because diagnostic accuracy decreased at the LAD territory (see Figure, Supplemental Digital Content 3, which demonstrates diagnostic performance of combined interpretation of IQ-SPECT images without and with CT-AC to predict FFR $\leq$ 0.80, http://links.lww.com/MD/C26). Further investigation is required to conclude whether or not FFR $\leq$0.80 is predictable using Tl-201 MPI-IQ-SPECT/CT. A multi-center validation cohort study is necessary to generalize our findings. Nonetheless, the present findings suggest that appropriately combined interpretations of MPI-IQ-SPECT without and with CT-AC enable the prediction of coronary lesions indicating clinically significant and insignificant FFR with some degree of certainty. Thus, we propose the novel application of CT-AC to MPI-IQ-SPECT for FFR prediction even in patients who are not obese.

### 4.6. Limitations

This study was limited by proceeding at a single center with a relatively small sample of patients. We could not completely assign all myocardial segments to the appropriate coronary artery perfusion territory. A relatively high proportion of our patients had previously undergone percutaneous coronary intervention. Although minimizing radiation doses during MPI is important, we did not attempt to reduce the Tl-201 dose.

## References

[1] Levine GN, Bates ER, Blankenship JC, et al. 2011 ACCF/AHA/SCAI Guideline for Percutaneous Coronary Intervention: a report of the American College of Cardiology Foundation/American Heart Association Task Force on Practice Guidelines and the Society for Cardiovascular Angiography and Interventions. Circulation 2011;124:e574–651.

[2] Pijls NH, Tanaka N, Fearon WF. Functional assessment of coronary stenoses: can we live without it? Eur Heart J 2013;34:1335–44.

[3] Klocke FJ, Baird MG, Lorell BH, et al. ACC/AHA/ASNC guidelines for the clinical use of cardiac radionuclide imaging–executive summary: a report of the American College of Cardiology/American Heart Association Task Force on Practice Guidelines (ACC/AHA/ASNC Committee to Revise the 1995 Guidelines for the Clinical Use of Cardiac Radionuclide Imaging). Circulation 2003;108:1404–18.

[4] Nakajima K, Matsuo S, Okuyama C, et al. Cardiac event risk in Japanese subjects estimated using gated myocardial perfusion imaging, in conjunction with diabetes mellitus and chronic kidney disease. Circ J 2012;76:168–75.

[5] Tanaka H, Takahashi T, Kozono N, et al. Prediction of flow-limiting fractional flow reserve in patients with stable coronary artery disease based on quantitative myocardial perfusion imaging. Am J Cardiol 2016;117:1417–26.

[6] Singh B, Bateman TM, Case JA, et al. Attenuation artifact, attenuation correction, and the future of myocardial perfusion SPECT. J Nucl Cardiol 2007;14:153–64.

[7] Dorbala S, Di Carli MF, Delbeke D, et al. SNMMI/ASNC/SCCT guideline for cardiac SPECT/CT and PET/CT 1.0. J Nucl Med 2013;54: 1485–507.

[8] Flotats A, Knuuti J, Gutberlet M, et al. Hybrid cardiac imaging: SPECT/CT and PET/CT. A joint position statement by the European Association of Nuclear Medicine (EANM), the European Society of Cardiac Radiology (ESCR) and the European Council of Nuclear Cardiology (ECNC). Eur J Nucl Med Mol Imaging 2011;38:201–12.

[9] Takahashi T, Tanaka H, Kozono N, et al. Characteristics of images of angiographically proven normal coronary arteries acquired by adenosine-stress thallium-201 myocardial perfusion SPECT/CT-IQ·SPECT with CT attenuation correction changed stepwise. Ann Nucl Med 2015;29:256–67.

[10] Masood Y, Liu YH, Depuey G, et al. Clinical validation of SPECT attenuation correction using x-ray computed tomography-derived attenuation maps: multicenter clinical trial with angiographic correction. J Nucl Cardiol 2005;12:676–86.

[11] Benkiran M, Mariano-Goulart D, Bourdon A, et al. Is computed tomography attenuation correction more efficient than gated single photon emission computed tomography analysis in improving the diagnostic performance of myocardial perfusion imaging in patients with low prevalence of ischemic heart disease? Nucl Med Commun 2015;36: 69–77.

[12] DePuey EG. Advances in SPECT camera software and hardware: currently available and new on the horizon. J Nucl Cardiol 2012;19: 551–81.

[13] Caobelli F, Kaiser SR, Thackeray JT, et al. IQ SPECT allows a significant reduction in administered dose and acquisition time for myocardial perfusion imaging: evidence from a phantom study. J Nucl Med 2014;55: 2064–70.

[14] Caobelli F, Thackeray JT, Soffientini A, et al. Feasibility of one-eighth time gated myocardial perfusion SPECT functional imaging using IQ-SPECT. Eur J Nucl Med Mol Imaging 2015;42:1920–8.

[15] Matsuo S, Nakajima K, Onoguchi M, et al. Nuclear myocardial perfusion imaging using thallium-201 with a novel multifocal collimator SPECT/CT: IQ-SPECT versus conventional protocols in normal subjects. Ann Nucl Med 2015;29:452–9.

[16] Takamura T, Horiguchi Y, Kanna M, et al. Validation of prone myocardial perfusion SPECT with a variable-focus collimator versus supine myocardial perfusion SPECT with or without computed tomography-derived attenuation correction. Ann Nucl Med 2015;29: 890–6.

[17] Okuda K, Nakajima K, Matsuo S, et al. Creation and characterization of normal myocardial perfusion imaging databases using the IQ·SPECT system. J Nucl Cardiol 2017;[Epub ahead of print].

[18] Konishi T, Nakajima K, Okuda K, et al. IQ-SPECT for thallium-201 myocardial perfusion imaging: effect of normal databases on quantification. Ann Nucl Med 2017;31:454–61.

[19] Cerqueira MD, Weissman NJ, Dilsizian V, et al. Standardized myocardial segmentation and nomenclature for tomographic imaging of the heart. A statement for healthcare professionals from the Cardiac Imaging Committee of the Council on Clinical Cardiology of the American Heart Association. Circulation 2002;105:539–42.

[20] Abidov A, Hachamovitch R, Hayes SW, et al. Are shades of gray prognostically useful in reporting myocardial perfusion single-photon emission computed tomography? Circ Cardiovasc Imaging 2009;2: 290–8.

[21] Pencina MJ, D'Agostino RBSr, D'Agostino RBJr, et al. Evaluating the added predictive ability of a new marker: from area under the ROC curve to reclassification and beyond. Stat Med 2008;27:157–72.

[22] Pijls NH, De Bruyne B, Peels K, et al. Measurement of fractional flow reserve to assess the functional severity of coronary-artery stenoses. N Engl J Med 1996;334:1703–8.

[23] Yanagisawa H, Chikamori T, Tanaka N, et al. Correlation between thallium-201 myocardial perfusion defects and the functional severity of coronary artery stenosis as assessed by pressure-derived myocardial fractional flow reserve. Circ J 2002;66:1105–9.

[24] Erhard I, Rieber J, Jung P, et al. The validation of fractional flow reserve in patients with coronary multivessel disease: a comparison with SPECT and contrast-enhanced dobutamine stress echocardiography. Z Kardiol 2005;94:321–7.

[25] Adjedj J, De Bruyne B, Floré V, et al. Significance of intermediate values of fractional flow reserve in patients with coronary artery disease. Circulation 2016;133:502–8.

[26] Herzog BA, Buechel RR, Katz R, et al. Nuclear myocardial perfusion imaging with a cadmium-zinc-telluride detector technique: optimized protocol for scan time reduction. J Nucl Med 2010;51:46–51.

[27] Chikamori T, Hida S, Tanaka N, et al. Diagnostic performance of a cadmium-zinc-telluride single-photon emission computed tomography system with low-dose technetium-99m as assessed by fractional flow reserve. Circ J 2016;80:1217–24.

[28] Tron C, Donohue TJ, Bach RG, et al. Comparison of pressure-derived fractional flow reserve with poststenotic coronary flow velocity reserve for prediction of stress myocardial perfusion imaging results. Am Heart J 1995;130:723–33.

[29] Caymaz O, Fak AS, Tezcan H, et al. Correlation of myocardial fractional flow reserve with thallium-201 SPECT imaging in intermediate-severity coronary artery lesions. J Invasive Cardiol 2000;12:345–50.

[30] Rieber J, Jung P, Erhard I, et al. Comparison of pressure measurement, dobutamine contrast stress echocardiography and SPECT for the evaluation of intermerdiate coronary stenoses. The COMPRESS trial. Int J Cardiovasc Intervent 2004;6:142–7.

[31] Hacker M, Rieber J, Schmid R, et al. Comparison of Tc-99m sestamibi SPECT with fractional flow reserve in patients with intermediate coronary artery stenoses. J Nucl Cardiol 2005;12:645–54.

[32] Ragosta M, Bishop AH, Lipson LC, et al. Comparison between angiography and fractional flow reserve versus single-photon emission computed tomographic myocardial perfusion imaging for determining lesion significance in patients with multivessel coronary disease. Am J Cardiol 2007;99:896–902.

[33] Förster S, Rieber J, Ubleis C, et al. Tc-99m sestamibi single photon emission computed tomography for guiding percutaneous coronary intervention in patients with multivessel disease: a comparison with quantitative coronary angiography and fractional flow reserve. Int J Cardiovasc Imaging 2010;26:203–13.

[34] Melikian N, De Bondt P, Tonino P, et al. Fractional flow reserve and myocardial perfusion imaging in patients with angiographic multivessel coronary artery disease. JACC Cardiovasc Interv 2010;3:307–14.

[35] Sahiner I, Akdemir UO, Kocaman SA, et al. Quantitative evaluation improves specificity of myocardial perfusion SPECT in the assessment of functionally significant intermediate coronary artery stenoses: a comparative study with fractional flow reserve measurements. Ann Nucl Med 2013;27:132–9.

[36] Jakljević T, Ruzić A, Bazdarić K, et al. Detection of myocardial ischemia in diabetic patients: the limitations of myocardial perfusion imaging. Coll Antropol 2012;36:821–6.

[37] Schaap J, Kauling RM, Boekholdt SM, et al. Incremental diagnostic accuracy of hybrid SPECT/CT coronary angiography in a population with an intermediate to high pre-test likelihood of coronary artery disease. Eur Heart J Cardiovasc Imaging 2013;14:642–9.

[38] Kamiya K, Sakakibara M, Asakawa N, et al. Cardiac magnetic resonance performs better in the detection of functionally significant coronary artery stenosis compared to single-photon emission computed tomography and dobutamine stress echocardiography. Circ J 2014;78:2468–76.

[39] Morishima T, Chikamori T, Hatano T, et al. Correlation between myocardial uptake of technetium-99m-sestamibi and pressure-derived myocardial fractional flow reserve. J Cardiol 2004;43:155–63.

[40] Ben Bouallègue F, Roubille F, Lattuca B, et al. SPECT myocardial perfusion reserve in patients with multivessel coronary disease: correlation with angiographic findings and invasive fractional flow reserve measurements. J Nucl Med 2015;56:1712–7.

[41] Motwani M, Motlagh M, Gupta A, et al. Reasons and implications of agreements and disagreements between coronary flow reserve, fractional flow reserve, and myocardial perfusion imaging. J Nucl Cardiol 2015; [Epub ahead of print].

[42] Malkerneker D, Brenner R, Martin WH, et al. CT-based attenuation correction versus prone imaging to decrease equivocal interpretations of rest/stress Tc-99m tetrofosmin SPECT MPI. J Nucl Cardiol 2007;14:314–23.

[43] Genovesi D, Giorgetti A, Gimelli A, et al. Impact of attenuation correction and gated acquisition in SPECT myocardial perfusion imaging: results of the multicentre SPAG (SPECT Attenuation Correction vs Gated) study. Eur J Nucl Med Mol Imaging 2011;38:1890–8.

[44] Sharma P, Patel CD, Karunanithi S, et al. Comparative accuracy of CT attenuation-corrected and non-attenuation-corrected SPECT myocardial perfusion imaging. Clin Nucl Med 2012;37:332–8.

[45] Sciagrà R. The expanding role of left ventricular functional assessment using gated myocardial perfusion SPECT: the supporting actor is stealing the scene. Eur J Nucl Med Mol Imaging 2007;34:1107–22.

[46] Danad I, Szymonifka J, Twisk JWR, et al. Diagnostic performance of cardiac imaging methods to diagnose ischaemia-causing coronary artery disease when directly compared with fractional flow reserve as a reference standard: A meta-analysis. Eur Heart J 2017;38:991–8.